Applied Acoustics 200 (2022) 109063

Contents lists available at ScienceDirect

Applied Acoustics

journal homepage: www.elsevier.com/locate/apacoust

Broadband high-efficiency meta-structures design by acoustic critical absorption effect

Li Bo Wang, Chang Wang, Yun Zhong Lei, Shao Kun Yang, Jiu Hui Wu *

School of Mechanical Engineering & State Key Laboratory for Strength and Vibration of Mechanical Structures, Xi'an Jiao Tong University, Xi'an 710049, China

ARTICLE INFO

Article history:
Received 12 April 2022
Received in revised form 16 August 2022
Accepted 6 October 2022

Keywords:
Sound absorption
Micro-perforated panel
Broadband and high-efficiency
Acoustic critical absorption effect
Unit arrangement

ABSTRACT

For resonant-type meta-structures with finite dimensions and consisting of multiple units, their sound absorption performance varies with the placement of the units. In order to reveal the physical mechanism of this phenomenon and obtain the structural design rules to achieve optimal sound absorption performance, the acoustic critical absorption effect is proposed in this paper. Based on this, a 50 mm thick meta-structure is proposed, which obtains an average sound absorption performance of 70 % from 1000 Hz to 2800 Hz. Compared with a structure of the same size but without considering the acoustic critical absorption effect, the sound absorption performance of the proposed meta-structure is increased by 30 %. The high agreement between finite element simulations and experimental results verifies the reliability of the conclusions. This work provides a potential avenue for enhancing noise reduction performance and reducing the dimension of the structures.

© 2022 Elsevier Ltd. All rights reserved.

1. Introduction

Sound absorption as an effective noise control [1–2] has always been one of the hotspots of acoustical research, and sound-absorbing materials have received widespread attention. For traditional materials such as porous materials [3–8], although satisfactory absorption performance can be obtained for high-frequency, they usually have a structural thickness equivalent to the working wavelength, which hampers their potential application in low-frequency. Micro-perforated panel [9–10] and resonant-cavity type [11] structures enable efficient low frequency sound absorption with small dimensions. However, the narrow-band characteristic is an obstacle for practical applications, and the dimensions needs to be further reduced. With ingenious structural design and special physical mechanisms[12], meta-structures [13–15] can achieve a smaller size and better sound-absorbing effect. Up to now, the researchers have proposed deep research from multiple angles and obtained mainly-two types of meta-structure: resonant-type meta-structures such as Helmholtz resonators [16], membrane-type meta-structures (MAMs)[17–23], coiling-up meta-structures [24–27], and Bragg scattering type meta-structures such as phononic metamaterials [28,29]. Among them, resonant-type meta-structure has become one of the current research interests for its low-frequency and efficient sound absorption performance in deep sub-wavelength dimensions. However, the narrow-band characteristics of the local resonance mechanism and limited structure size make it difficult to achieve broadband sound-absorption performance.

In order to get over the hump of the narrow-band characteristics of resonant-type meta-structures, two major ways are proposed in general. One way is to combine resonant-type structure and porous materials. Arjunan et al. [30] demonstrated a high-efficiency sound absorber in the low to medium frequency range by coupled micro-perforated panel with porous medium. Gao et al. [31] proposed a composite porous metamaterial (CPM) consisting in a porous polyurethane sponge with embedded multi-layer I-plates to obtain satisfactory absorption performance within 6.4 kHz. The other way is to focus on the arrangement of the absorption units, there can be divided into series-type and parallel-type. For series-type arrangements [32–34], the usual approach is to add a new unit in the vertical direction of the structural unit and increase a second-order peak while ensuring that the first-order sound absorption peak is almost unchanged by adjusting the acoustic impedance of the unit, to broaden the sound absorption band of the structure. Although this method can broaden the sound absorption frequency band, it significantly increases the structure's thickness. For parallel-type arrangements [35,36], it is realized by utilizing the cooperative coupling between the horizontally arranged units so that the sound absorption peak generated by the units is strictly coupled to form a broadband sound absorption effect. This method can broaden the absorption

* Corresponding author.
E-mail address: ejhwu@mail.xjtu.edu.cn (J.H. Wu).

https://doi.org/10.1016/j.apacoust.2022.109063
0003-682X/© 2022 Elsevier Ltd. All rights reserved.

band without increasing the structure's thickness. However, broadening the absorption band depends on the number of units and the degree of impedance matching for an acoustic structure with a limited size. Hence, there are high requirements for the arrangement of the units and space utilization.

For obtaining optimal sound absorption with limited structural dimensions, several works have been presented. Huang et al. [37] proposed coherently coupled weak resonances and demonstrated quasi-perfectly absorption performance with ultra-thin thickness can be obtained by exerting the coherent coupling effect among the imperfect components. Zhou et al. [38] presented the overdamped recipe and the reduced excessive response recipe and achieved the minimal thickness with satisfactory absorption performance required by the causality constraint. Some works also proposed new ideas to realize good absorption performance with a sub-wavelength scale. Ding et al. [39] presented meta-liner with metal foam achieves unanimously high-efficiency sound absorption from 800 Hz to 3200 Hz via a thin structure of 40 mm. Zhou et al. [40] present a design of a low-frequency perfect acoustic absorption metaporous composite with frequency tunability and the insensitivity to the incident angle based on a critical coupling mechanism. Gao et al. [41] used teaching–learning-based optimization algorithm to optimize a composite absorber, which could provide broadband sound absorption from 0 to 1.6 kHz. However, the relationship between the sound absorption performance and the unit arrangement has not attracted enough attention. In this paper, we present the acoustic critical absorption effect to reveal the general rule and the physical mechanism behind the optimal sound absorption performance of resonant-type meta-structures from the perspective of the unit layout. Moreover, based on the cross-sectional area of the meta-structures, the problem of optimizing the number of synergistic coupling units at different absorption bands is also analyzed in detail. In doing so, under the limited cross-sectional area of the meta-structure, by arranging as many resonant acoustic absorption units as possible at optimal locations in a parallel arrangement, instead of arranging multiple resonant units in series, it is possible to achieve a significant reduction in thickness and at the same time obtain broadband efficient acoustic performance.

The rest parts of the paper are organized as follows: section 2 employs the MPP model to describe the basic phenomenon and physical mechanisms of the acoustic critical absorption effect, and the finite element theory together with the modeling method are analyzed; section 3 explores three aspects of a single unit, a group of identical units and multiple groups of different units to reveal the general rules for obtaining the optimal sound absorption performance of the structure; section 4 gives a 24-unit meta-structure constructed with multiple micro-perforated panel (MPP) units and applied acoustic critical absorption effect is carried out to obtain 70 % average absorption performance at 1000 Hz-2800 Hz with the structure diameter is only 50 mm, which is 30 % improvement of absorption performance compared with the structure with the same scale but not apply acoustic critical absorption effect. The high coincidence between finite element simulation and experiment results verified the reliability of the conclusion. Finally, some important conclusions are made in section 5.

2. Description and calculation method of the acoustic critical absorption effect

2.1. The description of the acoustic critical absorption effect

To illustrate the acoustic critical absorption effect clearly, Fig. 1 shows two models composed of three identical micro-perforated panels (MPP) with back cavities but arranged in two different ways. The arrows in Fig. 1denotes the arrangement direction of the units. It is obvious that the units of model 1 are arranged in a uniform way along the circumference, while model 2 is arranged in a straight line along the structural radius, and the spacing between the two units is 5 mm. The hole diameter, the thickness of the perforated plate, perforation rate, and back cavity depth is 1 mm, 1 mm, 10 %, and 50 mm. The units in both models are perforated on one side. The other side is the bottom of the back cavity which can be regarded as an acoustically hard boundary. The schematic of the models is shown in Fig. 1. Noted that the absorption coefficient of the designed unit satisfies the perfect sound absorption in its limited absorption area according to Maa's formula [42]. The diameter of the incident area and the cross-sectional of the unit are 50 mm and 7 mm, respectively.

Fig. 2 illustrates the sound absorption performance of model 1 and model 2. It is observed that even though the unit parameters used in the two models are the same, the different arrangement leads to the apparent difference in sound absorption coefficients between the two models. In specific, model 1 produces a sound absorption peak with a maximum sound absorption coefficient of 0.86 at 1470 Hz, recorded as P_1, and its sound absorption coefficient is significantly greater than the sound absorption peak P_{21}, P_{22}, and P_{23} at 1400 Hz, 1450 Hz, and 1490 Hz generated by model 2.

Fig. 3 illustrates the surface relative acoustic impedance of model 1 and model 2. It shows that the surface relative acoustic reactance Im(z) of model 1 and model 2 crossed zero at 1400 Hz and 1470 Hz respectively, which is just corresponds to the positions of sound absorption peaks P_1 and P_{21} shown in Fig. 1. Furthermore, the surface relative acoustic resistance Re(z) of two models at P_1 and P_{21} are 0.81 and 0.66 respectively, which shows model 1 has smaller surface acoustic reflection than model 2, so more sound energy is absorbed, resulting in better sound absorption effect. Noted that compared with model 1, Re(z) and Im(z) of model 2 produce two local valleys at the positions of P_{22} and P_{23}, so that the impedance matching characteristics at these two positions are better than those at other positions in the local area, thus producing two absorption peaks as shown in Fig. 2. However, since the Im(z) of these two is much larger than 0, their absorption coefficients are weaker than P_{21}. Moreover, the surface relative surface acoustic impedance amplitude $|z|$ corresponding to the three peaks of model 2 gradually increases, which is related to the average sound pressure $|p|$ and average sound particle velocity $|v|$ on the surface of the structure.

In order to further investigate the acoustic critical absorption effect and explain the sound absorption performance shown in Fig. 2, Fig. 4 illustrates the distribution of the air particle velocity of model 1 and model 2 at the location of their absorption peak in the X-Y direction. The direction of the arrow indicates the velocity direction of the acoustic particle, and the length of the arrow indicates the velocity magnitude. It shows that for P_1 generated by model 1, by evenly arranging the sound absorption units, the incident sound particles can be evenly absorbed in the effective sound absorption area of the units to achieve a smaller reflection and higher sound absorption coefficient. For P_{21}, P_{22}, and P_{23} produced by model 2, it is clear that although the units of model 2 are the same as those of model 1, the effective sound absorption area is different, and the effective sound absorption area decreases with the increase of peak frequency. Furthermore, the amplitude of the air particle velocity of model 2 decreases with the increase in the frequency of absorption peaks. Thus, since the velocities of the units in model 2 are weakened with the increase of the frequency while the incident sound pressure is kept constant, the surface relative impedance of model 2 will increase with increasing frequency according to$|z| = |p|/|v|$, which is coincidence with the phenomenon shown in Fig. 3.

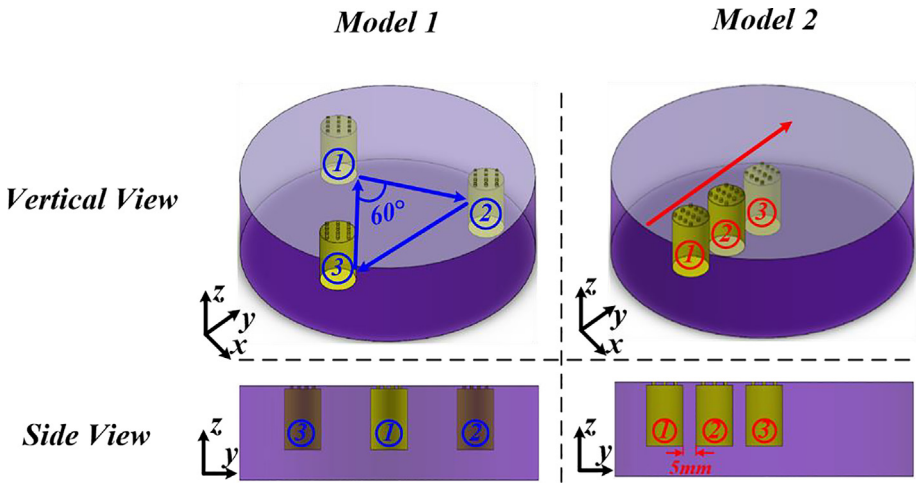

Fig. 1. Schematic of model 1 and model 2.

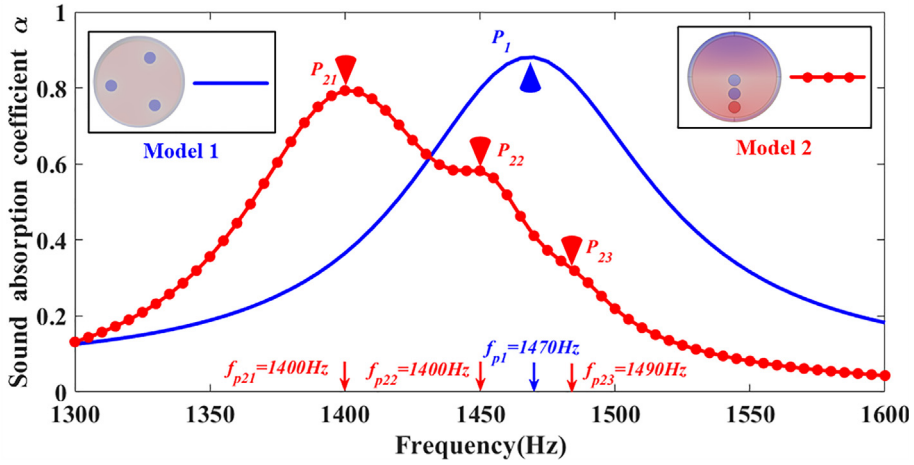

Fig. 2. Sound absorption performance of model 1 and model 2.

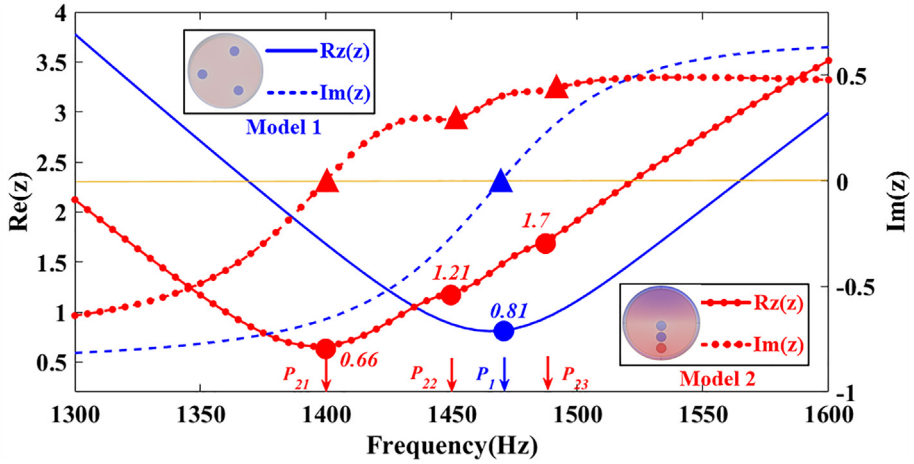

Fig. 3. The surface relative acoustic impedance of model 1 and model 2.

In summary, the uniform arrangement of multiple identical units can weaken the coupling between units and maximize the effective absorption area, thus obtaining good acoustic performance. This phenomenon of achieving optimal sound absorption through the rational arrangement of multiple sound absorption subunits is called the acoustic critical absorption effect. This effect

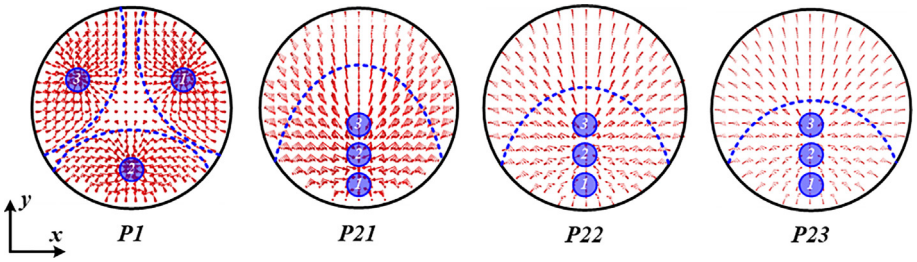

Fig. 4. The air particle velocity of model 1 and model 2 in the X-Y direction.

aims to reveal the general rule of unit layout to achieve the optimal sound absorption performance in the case of parallel arrangement of units.

2.2. Modeling and finite element calculation

2.2.1. Geometrical model

The study is carried out by employing the commercial software COMSOL Multiphysics™ 5.5. The geometric model consists of three parts, as shown in Fig. 5: The upper part is a cylinder as the sound incident region with a diameter and length of 100 mm, and the lower part of the model is a cylinder as a back cavity with a diameter of 12 mm and a length of 100 mm. For micro-perforated panels at the junction of two cylinders, the hole number, hole diameter, thickness of perforated plate, perforation rate, and back cavity depth are 16, 1.2 mm, 2 mm, and 3 %.

2.2.2. Boundary conditions and elements setting

Note that this work uses the 'internal perforated plate' option in the 'pressure acoustics' module instead of the 'thermal viscosity acoustics' module when calculating the perforated plate sound absorption to reduce the calculation time. Therefore, the model's overall boundary conditions and elements setting are as follows: The sound incident region and the back cavity are 'pressure acoustic' modules, and the side walls and bottom are set as 'acoustically hard boundaries.' The top of the incident area is set with 'plane wave radiation' as the sound incident surface, the sound wave direction is vertical downward, and the amplitude is 1 Pa. The junction area of the incident area and the back cavity is set as an 'internal perforated plate.'.

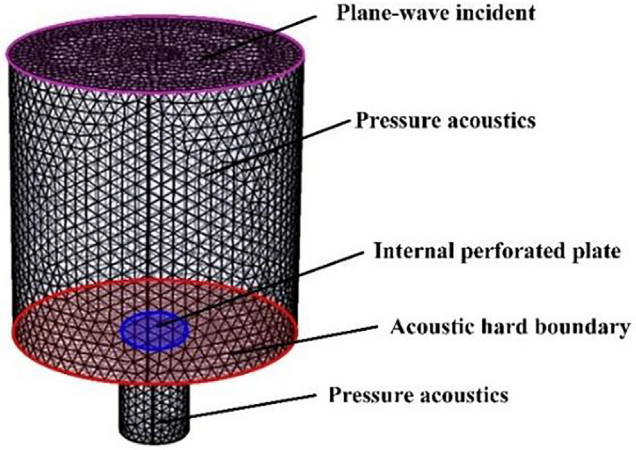

Fig. 5. Specific setting schematic of the unit.

2.2.3. Post processing

Assuming that the incident plane wave passing along the z-axis in the positive direction to the negative direction can be expressed as:

$$p(z,t) = p_{ia}e^{i(\omega t - kz)} \tag{2}$$

where p_{ia} is the amplitude of the incident wave, $k = \frac{\omega}{c_0}$ is the wave number. ω and c_0 represent angular frequency and sound velocity of the air.

Then, the particle velocity is written by.

$$v(z,t) = \frac{p_{ia}}{\rho_0 c_0} e^{i(\omega t - kz)} \tag{3}$$

where ρ_0 is the density of the air.

Suppose a sufficiently small volume element is taken in the sound field with the mass, density, volume, and pressure being m,ρ_1, V_1 and P_1. As the disturbance of the sound wave makes the volume of the element become V_2, the density becomesρ_2, and the pressure becomes P_2, the pressure difference generated in this process is$p = P_1 - P_2$, and the kinetic and potential energy gained by this volume element is.

$$E_k = \frac{1}{2}(\rho_1 V_1)v^2$$

$$E_p = \frac{1}{2}p(V_2 - V_1) = \frac{1}{2}p\frac{\rho_1 - \rho_2}{\rho_1 \rho_2}m \tag{5}$$

It can be deduced from the equation of state of ideal medium that.

$$dP = c_0^2 d\rho \tag{6}$$

Then we can obtain that.

$$p = (\rho_1 - \rho_2)c_0^2 \tag{7}$$

Substitute Eq. (7) into Eq. (5), the potential energy of the element can be rewritten as:

$$E_p = \frac{1}{2}\frac{p^2}{\rho_1 c_0^2}V_1 \tag{8}$$

The total sound energy can be obtained by adding Eq. (4) and Eq. (8) together.

$$E = \frac{1}{2}V_1\rho_1\left(v^2 + \frac{p^2}{\rho_1^2 c_0^2}\right) \tag{9}$$

The instantaneous value of the element sound energy can be obtained by taking the real part of Eq. (2) and Eq. (3) into Eq. (9)

$$E = V_1\frac{p_{ia}^2}{\rho_1 c_0^2}\cos^2(\omega t - kz) \tag{10}$$

The average sound energy for a period of the element is obtained as.

$$\bar{E} = \frac{1}{T}\int_0^T V_1 \frac{p_{ia}^2}{\rho_1 c_0^2}\cos^2(\omega t - kz)dt \tag{11}$$

where $T = \frac{2\pi}{\omega}$.

According to the definition, the average sound power density of the element can be written as.

$$\varepsilon = \frac{p_{ia}^2}{2\rho_1 c_0^2} \tag{12}$$

The sound intensity of the element is.

$$I = \varepsilon c_0 = \frac{p_{ia}^2}{2\rho_1 c_0} \tag{13}$$

Therefore, in the case where both the incident medium and the transmission medium are air in the finite element calculation, the incident, reflected, and transmitted sound energy can be expressed as.

$$E_{in} = \iint_{S_1} \frac{|p_{in}|^2}{2\rho_0 c_0} dS \tag{14}$$

$$E_{ref} = \iint_{S_1} \frac{|p - p_{in}|^2}{2\rho_0 c_0} dS \tag{15}$$

$$E_{out} = \iint_{S_2} \frac{|p|^2}{2\rho_0 c_0} dS \tag{16}$$

where S_1 and S_2 are the cross section in the incident and transmission medium perpendicular to the direction of sound propagation, respectively. p_{in} is the incident complex sound pressure.

Therefore, the sound absorption coefficient and reflection coefficient can be given as:

$$\alpha = 1 - \frac{E_{ref}}{E_{in}} - \frac{E_{out}}{E_{in}} \tag{17}$$

$$r = \frac{E_{ref}}{E_{in}} \tag{18}$$

Thus, the incident sound energy, reflection sound energy and sound absorption coefficient can be expressed as 'intop1(abs(pin)^2)', 'intop1(abs(acpr.p_t-pin)^2)' and '(1- intop1(abs(pin)^2)-intop1(abs(acpr.p_t-pin)^2))' in COMSOL. 'intop1′ is the area fraction of the top surface of the top cylinder, 'acpr.p_t' and 'pin' are sound pressure at the integrating surface and incident sound pressure.

2.2.4. Mesh and calculation errors

In order to compare the accuracy of the results after using the simplified model, Fig. 6 shows the sound absorption of the model using the 'thermal viscous module' and the simplified model using the coarse, conventional and refined mesh division. For the model applied to the 'thermal viscous module,' the maximum size of the mesh inside the small hole is $d_i/6$, and the minimum size is $d_v/2$, where d_i is the diameter of the small hole,$d_v = \sqrt{2\mu/\rho_0\omega}$. Other parts adopt conventional mesh division. Noted that since the trend of sound absorption performance above 500 Hz is stable and tends to 0, and the computational volume of the model increases significantly with the increase of frequency, in order to balance the computational cost and model reliability, Fig. 6 gives the sound absorption performance of models in the range of 300–1000 Hz. Therefore, the elements of those cases are 112427, 548, 1508, and 3630, respectively. It is clear from Fig. 6(a) that for the simplified models using 'internal perforated panel,' the difference between the results of the simplified and complex models gradually decreases, but the difference is not significant. In order to obtain the errors of the simplified models using the coarse, conventional and refined mesh division, the error function is constructed as:

$$error = \frac{\int_{f_L}^{f_H}\left(\bar{\alpha}_{simp} - \bar{\alpha}_{comp}\right)^2}{\int_{f_L}^{f_H}\left(\bar{\alpha}_{comp}\right)^2} \times 100\% \tag{19}$$

where $[f_L, f_H]$ is the frequency range, $\bar{\alpha}_{simp}$ and $\bar{\alpha}_{comp}$ is the average sound absorption coefficient of the simplified model and the complex model.

The errors of the simplified model using the coarse, conventional and refined mesh division are 3.6 %, 3.5 %, and 2.5 %, respectively. All of them are small enough. On the other hand, the computing time of the complex model and the simplified model using the coarse, conventional and refined mesh division are 18774 s, 74 s, 82 s, and 96 s, respectively. Therefore, considering the computational error and computational time, the subsequent finite element simulations are performed using a refined model with conventional meshing predefined by the software.

3. Optimization of absorption performance based on acoustic critical absorption effect

In order to obtain optimal sound absorption performance, the absorption performance optimization is obtained from three

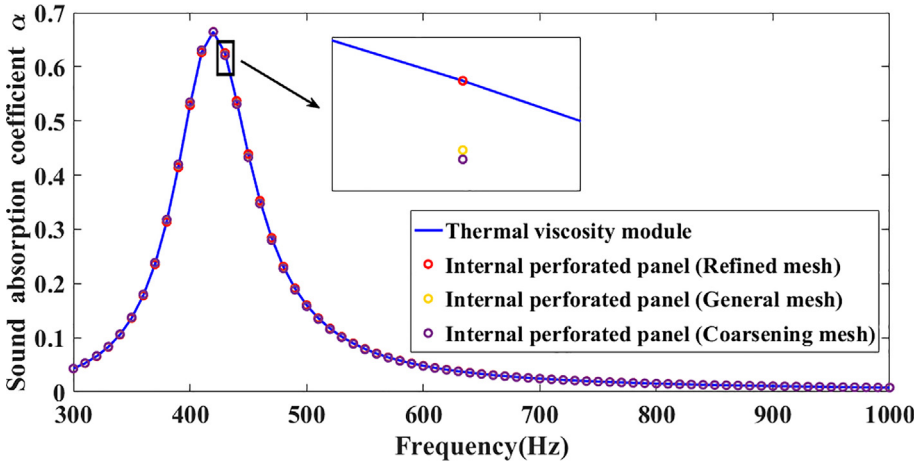

Fig. 6. Comparison of sound absorption results between the complex model using thermal viscosity module and the simplified model using an internal perforated panel.

aspects: the optimization of single unit, a group of identical units and multiple groups of different units.

3.1. Optimization of single unit

For making the study more general, we set up case 1, where the absorption peak is located at a relatively low frequency, and case 2, where it is located at a relatively high frequency, and investigated the effect of the placement of both on the absorption performance. The structural parameters for the two cases are shown in Table 1, in which S_0, S, n, d, t, and H are incident area, cross-sectional area of absorber, number of perforations, diameter of perforations, depth of perforations and the depth of the back cavity.

In order to describe the overall sound absorption performance of the structure in the investigated frequency range, the average sound absorption coefficient is introduced and can be written as:

$$\bar{\alpha} = \frac{\sum_{i=1}^{N} \alpha_i}{N} \tag{20}$$

where N is the number of frequency points under investigation, which can be expressed as $(f_H\text{-}f_L)/s$, where $[f_L, f_H]$ is the frequency range and s = 5 Hz is the step size of the finite element simulation.

Fig. 7 illustrates the variation of the average sound absorption coefficient and position of the absorption peak with different placements of the unit of case 1 and case 2. In both cases, it shows that the closer the unit's placement to the edge, the lower the location of its peak absorption frequency. Furthermore, the movement of the absorption peak is more pronounced in case 2 compared to case 1 where the absorption peak locates on relative lower frequency. Specifically, the absorption peak of case 1 moves from 1460 Hz to 1430 Hz when the unit moves from center to edge, the similar circumstance occurs in case 2 which the absorption peak moves from 1835 Hz to 1770 Hz. Another noteworthy phenomenon is that the average absorption coefficient of both cases is weakened with the unit moving to the edge of the structure. Moreover, compared with case 1, the average absorption coefficient of case 2 is more obviously affected by the placement of the unit.

Fig. 7(b) shows the sound absorption performance with the surface relative acoustic impedance of case 1 when the unit is arranged at the center and the edge of the structure. Compared to the cell arranged at the edge, when the unit is placed at the center, the surface relative acoustic reactance Im(z) crosses 0 at higher frequencies, and the surface relative acoustic resistance Re(z) is closer to 1. Thus, the peak generated by the local resonance generates a relatively higher absorption coefficient and frequency range. Fig. 7(c) illustrates a similar tendency to Fig. 7(b). For case 2, since the surface's relative acoustic impedance change is more evident than that in case 1, with the unit arranged from center to edge, the absorption performance changes more dramatically, and the absorption coefficient of absorption peak sharply decreased from 0.96 to 0.6.

Therefore, for a one-unit arrangement, the frequency of absorption peak and the sound absorption coefficient increase with the unit closer to the center of the structure. This phenomenon becomes more and more evident as the frequency increases.

3.2. Optimization of a group of identical units

Then, the optimization of a group of identical units is investigated. We still set the absorption units to the two cases shown in Table 1 and increase the number of units at equal distances along the diameter of the structure to reveal the effect of the number of absorption units with the same parameters on the sound absorption performance of the structure.

Fig. 8 illustrates the sound absorption performances with different quantities of units in case 1 and case 2. Fig. 8(a) shows the average absorption coefficient and location of absorption peak with different quantities of units in case 1 and case 2. It is obvious that the location of the absorption peak moves to a higher frequency with the increase of the number of units in both cases, and this tendency is more significant in case 2 than in case 1. Specifically, with the unit number increasing from 1 to 4, the location of the absorption peak moves from 1435 Hz to 1465 Hz. In contrast, the absorption peak changes from 1775 Hz to 1845 Hz, which indicates that the higher the sound absorption frequency range of the structure, the more sensitive the sound absorption performance is to changes in the number of units. On the other hand, with the increase in the number of units, $\bar{\alpha}$ increases first and then decreases and reaches the maximum when the number of units is 3 in both cases.

Fig. 8(b) illustrates the sound absorption performance and surface relative impedance of case 2 when the number of units is two, three, and four. It is shown that when the number of the units is two and three, there are double absorption peaks, while the number of the absorption peak becomes only one again when the number of units is four. From the surface relative impedance curve, it can be seen that when the number of units is two and three, for Im(z), each of them have a point crossed zero and the other point close to zero, therefore generating two resonant-type absorption peaks. Furthermore, since the Re(z) at their points are different, the degree of sound energy reflected on the surface of the structure is also different, the closer Re(z) is to 1, the less sound energy reflected by the structure, the better the sound absorption performance.

In order to describe the sound absorption phenomenon more clearly, Fig. 9 illustrates the air particle velocity with different units in case 2. As shown in Fig. 9(a), at the first absorption peak, the unit close to the edge absorbs more sound energy, while both units play a role at the second peak. Furthermore, the structure absorbs more sound energy at the second sound absorption peak, so the sound absorption performance produced by the structure at the second peak is better. A similar circumstance occurs when the number of units is three, as shown in Fig. 9(b). The absorption performance at the second peak is almost perfect since almost all the units absorb the sound energy.

After investigating the influence of the number in a group of units on sound absorption performance, the effect of the arrangement of a group of units on sound absorption performance will be studied. We place the three units in the position shown in Fig. 10 and draw the average sound absorption coefficient and the position of sound absorption peak in different arrangements ways in the two cases. It is clear that with the change of the arrangement ways, the average absorption coefficient in case 2 changes more significantly than in case 1. Furthermore, among

Table 1
Structural parameters of the two cases used in calculation.

Case	S_0(mm^2)	S(mm^2)	n	d(mm)	t(mm)	H(mm)
Case 1	100	36	42	1	1	50
Case 2	100	36	42	1	1	38

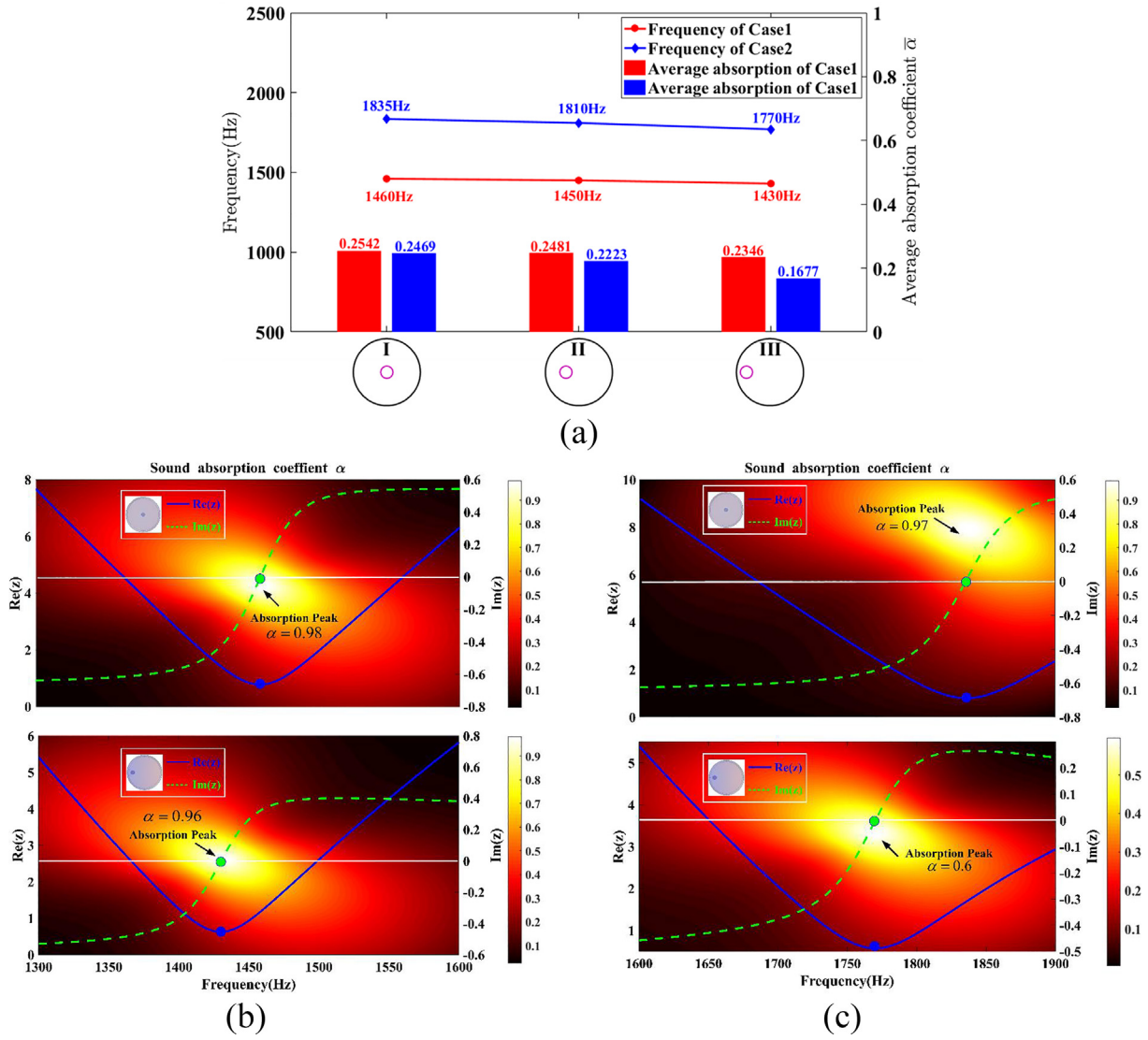

Fig. 7. Sound absorption performance with different positions of the unit. (a) average absorption performances and location of absorption peaks of case 1 and case 2 when the unit is arranged at the center an edge of the structure; (b) sound absorption coefficient and surface relative acoustic impedance of case 1; (c) sound absorption coefficient and surface relative acoustic impedance of case 2.

the four arrangements, the first way of unit arrangement as in Fig. 10, i.e., close arrangement along one side of the radius direction, has the worst sound absorption performance. In contrast, the other three ways of uniform arrangement have a better effect. This phenomenon can be attributed to the unit's effective sound absorption area, as Fig. 4 shows. Because the uniform arrangement of the units can have a larger effective sound absorption area than the centralized arrangement of the units, it can absorb more sound energy and thus have better sound absorption performance.

In summary, the sound absorption performance of multiple absorption units in the uniform arrangement is better than that in a close arrangement, which becomes more evident with the increased sound-absorbing frequency. In addition, in the form of uniform arrangement, the effect of uniform arrangement in the circumferential direction is better than that of uniform arrangement in the radial direction.

3.3. Optimization of multiple groups of different units

For multiple groups of different units, we set three groups, each consisting of three identical units evenly arranged along the circumference. The specific parameters of each group are shown in Table 2, in which S_0, S, n, d, t and H are the incident area, the cross-sectional area of the absorber, number of perforations, the diameter of perforations, depth of perforations and the depth of the back cavity.

Fig. 11 illustrates the sound absorption performance with multiple groups of different units. Since there are three groups of units with different structural parameters, three peaks are generated, as shown in the figure for *P*1, *P*2, and *P*3, which are generated by the first, second, and third groups, respectively. There are three cases depending on the radial arrangement of the units along the structure. Case 1 denotes when the three groups of sound-absorbing units are arranged in the radius direction from outside to inside as group 1, group 3, and group 2. Case 2 denotes when the three groups of sound-absorbing units are arranged in the radius direction from outside to inside as group 2, group 1, and group 3. Case 3 denotes when the three groups of sound-absorbing units are arranged in the radius direction from outside to inside as group 3, group 2, and group 1. The solid blue line, the dashed red line, and the dotted green line represent the sound absorption performance of case1, case 2, and case 3. It is shown that the solid blue

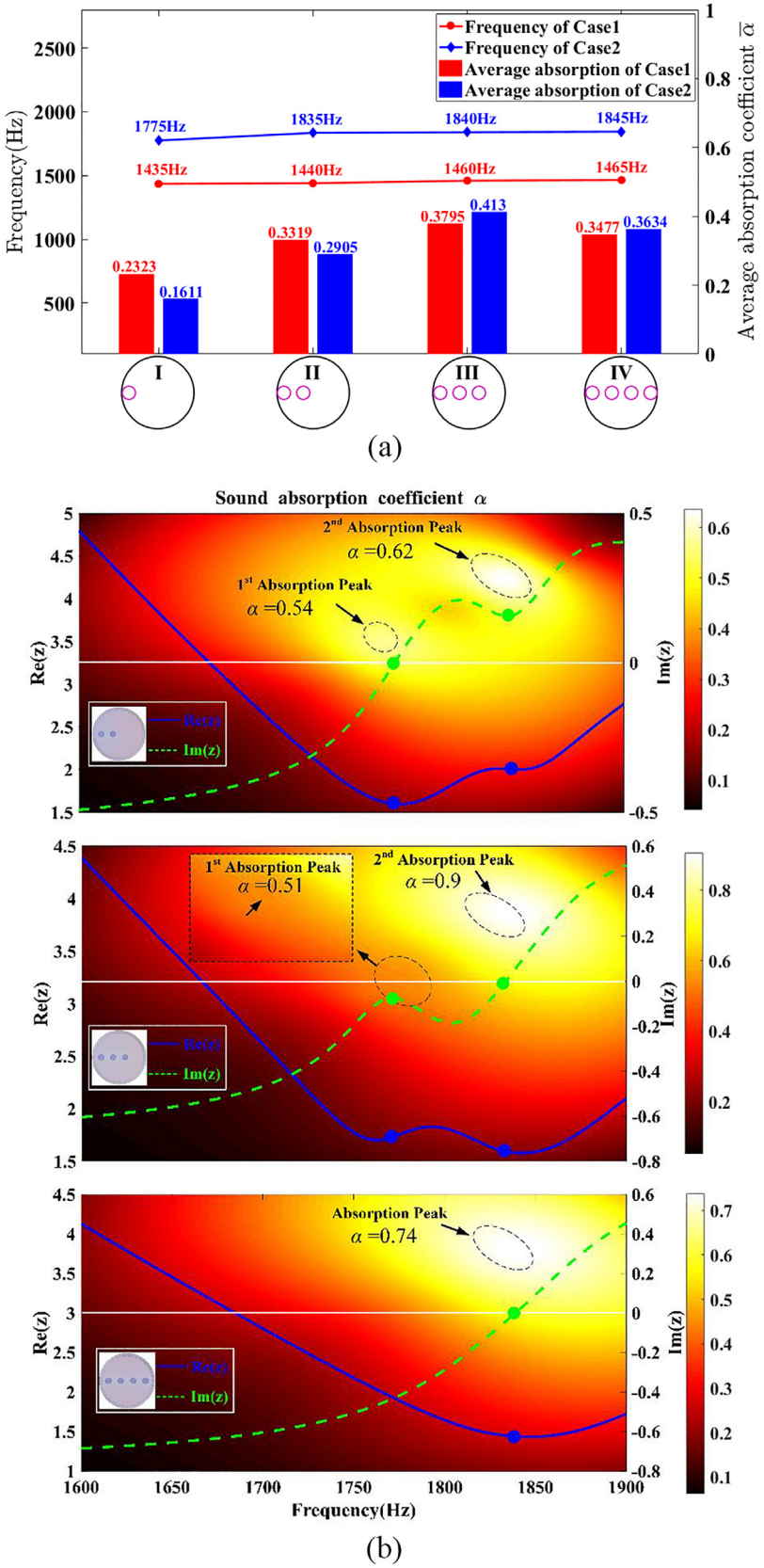

Fig. 8. Sound absorption performance with the different number of units. (a) average absorption performances and location of absorption peaks of case 1 and case 2 when the unit is arranged at the center an edge of the structure; (b) sound absorption coefficient and surface relative acoustic impedance of case 2.

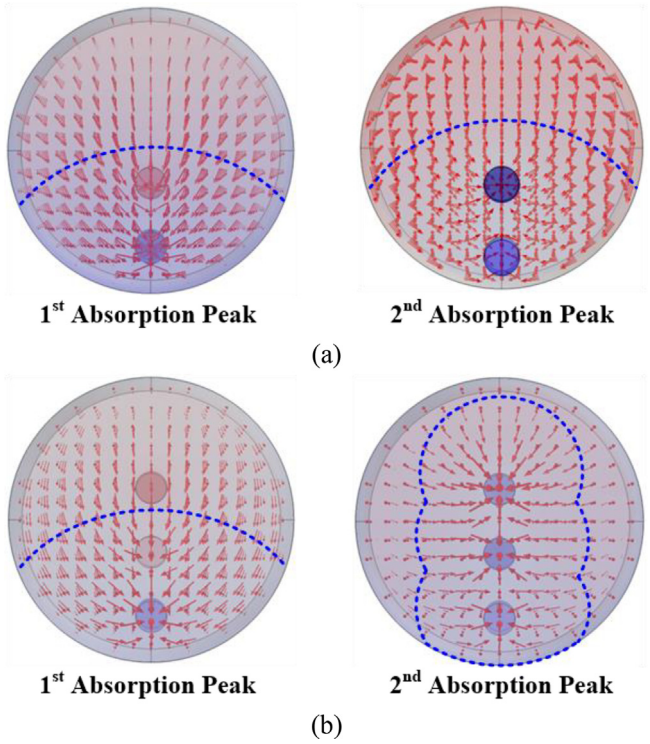

Fig. 9. The air particle velocity with different number of units. (a) Case 2 with 2 units; (b) Case 2 with 3 units.

line has the highest average absorption coefficient. Therefore, relatively good absorption performance is obtained by arranging the units that produce low-frequency absorption peaks outside the structure and those that produce high-frequency absorption peaks on the middle side. Furthermore, it can be seen that the alignment of the unit combination is different, resulting in a slightly different location of the absorption peak. This difference becomes more and more evident as the frequency of the absorption peak increases.

Therefore, the units with lower peak absorption frequencies should be arranged on both sides of the acoustic structure to obtain satisfactory sound absorption performance. The units with higher peak absorption frequencies should be arranged in the middle of the acoustic structure.

4. Experiment and discussion

4.1. Experimental set up

In order to verify the correctness of the acoustic critical absorption effect and obtain broadband high-efficiency sound absorption performance, Fig. 12 illustrates the schematic of 4 meta-structures used in the experiment. Case 1 and case 2 are two meta-structures composed of 24 units. The specific parameters of the units used in case 1 and case 2 are listed in Table 3 and 4. *L*, *R*, *n*, *d*, *t*, and *H* are the side length of the absorber, the radius of the absorber, number of perforations, the diameter of perforations, depth of perforations, and the depth of the back cavity. Case 3 and case 4 are two meta-structures with 6-unit. The specific parameters of the units used in case 1 and case 2 are listed in Table 5 and 6.

It should be highlighted that in case 1 and case 3, each group of units was arranged evenly, and the units of different groups were arranged according to the frequency of their absorption peaks. Specifically, the group producing high-frequency peaks was arranged in the middle of the structure, and the groups producing low and medium frequencies were arranged on the inner and outer sides of the structure. In case 2 and case 4, the units of the same group are arranged in a tight arrangement, and the units of different groups are arranged next to each other. The horizontal distance between each unit is 5 mm, and the longitudinal distance is 10 mm.

Fig. 13 illustrates the four meta-structures used in the experiment. All samples are made by 3D printing. The material of samples is photopolymer. The wiiboox light two pro is applied as the 3D printer. The specific settings of the main parameters are as follows: The perforated panel part of all samples has a layer thickness of 0.1 mm, and the lifting distance, lifting speed, and retraction speed of the z-axis are 0.2 mm, 0.2 mm/s, and 0.2 mm/s, respectively. The rest of the samples have a thickness of 0.2 mm per layer, and the lifting distance, lifting speed, and retraction speed of the z-axis is 1 mm, 1 mm/s and 1 mm/s, respectively. The diameter and the thickness of case 1 and case 2 are 99 mm and 50 mm. The side length and thickness of case 3 and case 4 are 49.5 mm and 35 mm.

The main purpose of designing two groups of samples (group 1 contains case 1 and case 2, group 2 contains case 3 and case 4) are as follows: first, to verify that the application of the acoustic critical absorption effect can enhance the broadband efficient sound absorption performance without changing the dimensions of the

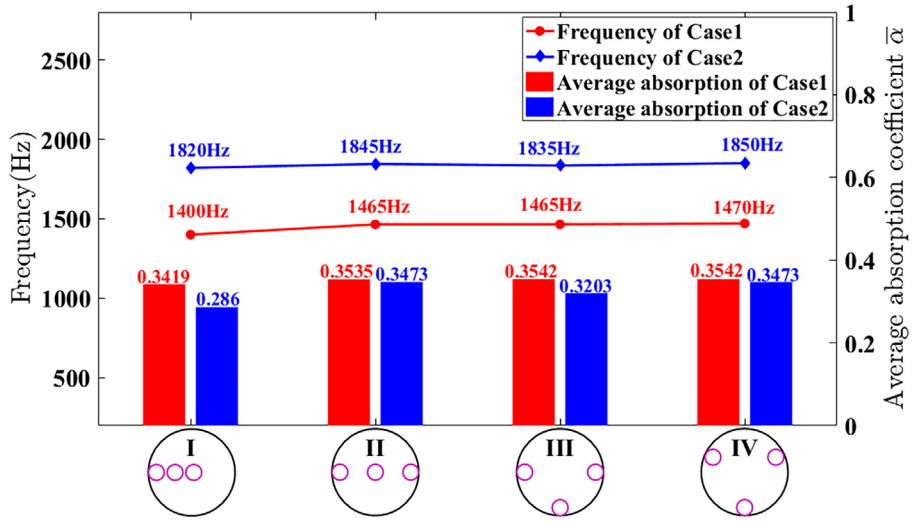

Fig. 10. Sound absorption performance with different arrangement of the units.

Table 2
Structural parameters of the three groups used in calculation.

Group	S_0(mm^2)	S(mm^2)	n	d(mm)	t(mm)	H(mm)
Group 1	100	36	12	1	1	37
Group 2	100	36	12	1	1	23
Group 3	100	36	12	1	1	14

meta-structure; second, to verify that the significance of the acoustic critical absorption effect increases with increasing frequency; and finally, to verify the generality of the acoustic critical absorption effect, i.e., it is applicable to structures with different cross-sectional shapes.

Fig. 14 illustrates the sound impedance tubes for obtaining the sound absorption coefficient of samples. Fig. 14(a) shows the B&K type-4206 impedance tube system. The diameter of the impedance tube is 100 mm, and the cut-off frequency is 1600 Hz. Fig. 14(b) shows the square impedance tube system. The side length of the impedance tube is 50 mm, and the cut-off frequency is 3200 Hz. The actuator is driven by a power amplifier (B&K 2716) that amplifies the sweep signal produced by the D/A converter (B&K 3560-C). An A/D converter acquires hydrophones signals. A B&K Pulse Lab shop program controls both A/D and D/A processes.

Table 3
Structural parameters of the units in case 1.

No.	R(mm^2)	n	d(mm)	t(mm)	H(mm)
1,3,5	8	16	1	1	14.5
2,4,6	8	16	1	1	12
7,13,19	6	12	1	1	50
10,16,22	6	12	1	1	44
9,15,21	6	12	1	1	37
12,18,24	6	9	1	1	31
11,17,23	6	16	1	1	27
8,14,20	6	16	1	1	23

The construction of the two impedance tube test platforms and the test process are carried out by ISO 10534-2:1998(E) [43], and the accuracy of the sound tube test results has been verified in the previous works [32,44]. Note that both samples' sound absorption performance is applied by the two microphones transfer function method. The two microphones behind the sample are not used in this experiment. The primary purpose of being placed on the acoustic tube is to keep the microphone mounting holes sealed to avoid sound leakage and to keep the inner surface of the sound pipe smooth. In the experiment, due to the limitation of structural size, case 1 and case 2 are measured by the impedance tube shown

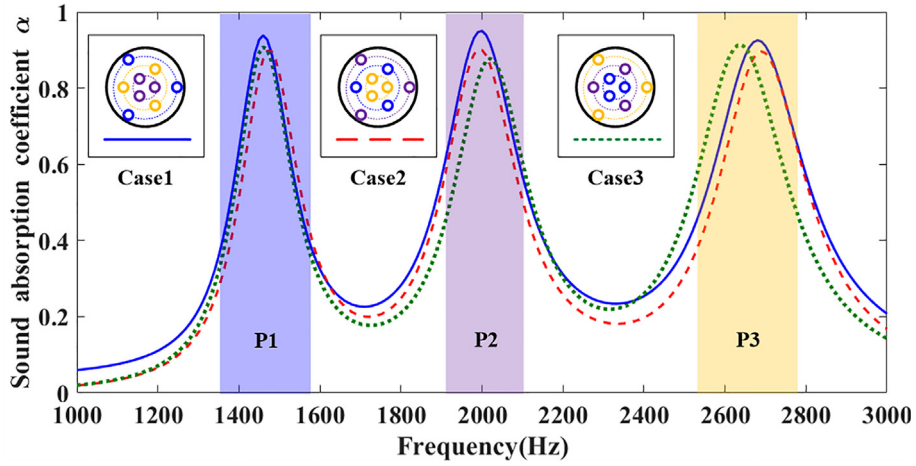

Fig. 11. Sound absorption performance with multiple groups of different units.

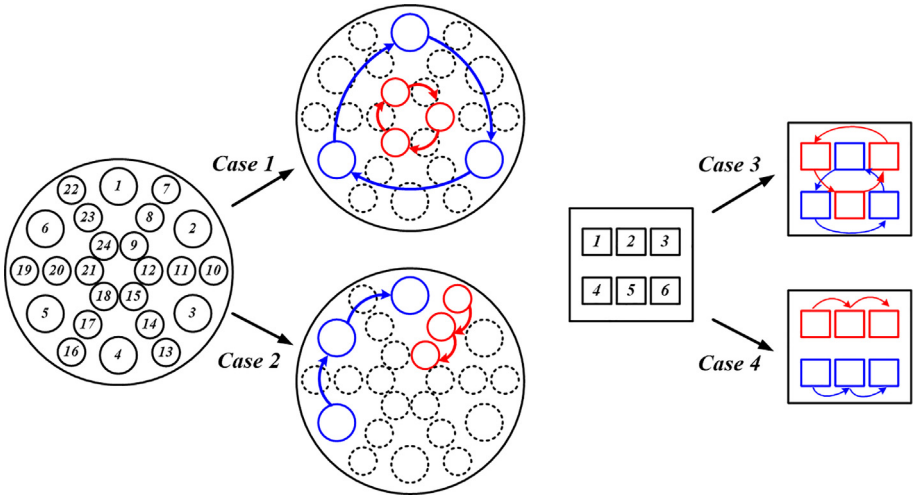

Fig. 12. Schematic of two cases of meta-structures. The arrangement of case 1 and case 3 considered the acoustic critical absorption effect; the arrangement of case 2 and case 4 without considering the acoustic critical absorption effect.

Table 4
Structural parameters of the units in case 2.

No.	R(mm^2)	n	d(mm)	t(mm)	H(mm)
1,2,3	8	16	1	1	14.5
4,5,6	8	16	1	1	12
7,8,9	6	12	1	1	50
10,11,12	6	12	1	1	44
13,14,15	6	12	1	1	37
16,17,18	6	9	1	1	31
19,20,21	6	16	1	1	27
22,23,24	6	16	1	1	23

Table 5
Structural parameters of the units in case 3.

No.	L(mm^2)	n	d(mm)	t(mm)	H(mm)
1,3,5	10	16	1	1	25
2,4,6	10	16	1	1	30

Table 6
Structural parameters of the units in case 4.

No.	L(mm^2)	n	d(mm)	t(mm)	H(mm)
1,2,3	10	16	1	1	25
4,5,6	10	16	1	1	30

Fig. 13. Pictures of meta-structures used in the experiment.

in Fig. 14 (a), and case 3 and case 4 are measured by the impedance tube shown in Fig. 14 (b). In order to prevent sound leakage, the dimensions of the samples closely fit the inner diameter of the impedance tubes, with an error of 1 %. Furthermore, the gaps between the samples and impedance tubes are sealed with acoustic insulation rubber to ensure maximum fit and minimum sound leakage from the samples.

Note that since the cut-off frequency of the impedance tube shown in Fig. 14(a) is 1600 Hz, the sound absorption performance of case 1 and case 2 after 1600 Hz may not be accurately measured. In order to verify the sound absorption performance of case 1 and case 2 from 1600 Hz to 2800 Hz, we designed the sound absorption experiment in the anechoic room. The schematic diagram of the experiment platform is shown in Fig. 15. The sample baffle is placed on the experimental platform. The loudspeaker is placed 1 m in front of the center of the sample. The loudspeaker gradually emits a sweeping signal, and microphones record the sound pressure levels at different frequencies at 0.1 m, 0.15 m, and 0.2 m in front of the sample; then, the sample is reversed. The sound waves are directly incident to the surface of the baffle, which can be regarded as an absolute hard boundary at this time. The sound pressure level at the same position is recorded; finally, according to the sound pressure level of the two measurements, the sound absorption performance of the metamaterial sample can be obtained indirectly. Then, combining the results of 1000 Hz-1600 Hz tested by impedance tube with the results of 1600 Hz-2800 Hz measured by the anechoic chamber, we get the sound absorption performance of case 1 and case 2 from 1000 Hz to 2800 Hz.

4.2. Results and discussions

Fig. 16 illustrates the sound absorption performance of 4 meta-structures. Fig. 16(a) shows the sound absorption performance of case 1 and case 2 from 1000 to 2800 Hz. The experiment results obtained by the impedance tube experiment are in good agreement with the finite element simulation results in the range of 1000 Hz-1600 Hz, which verifies the correctness of the results. In the frequency band greater than 2000 Hz, the sound absorption performance of the meta-structures is obtained by an anechoic room experiment. Although there are some differences between the finite element simulation results and experiment results, the trend of the experiment results of the sound absorption performance in the two cases is consistent with the trend of the finite element simulation results. The difference can be attributed to the processing error of the sample and the interference of reflected sound waves from the test desk. It can be observed that both cases produced 8 absorption peaks, corresponding to the 8 groups of

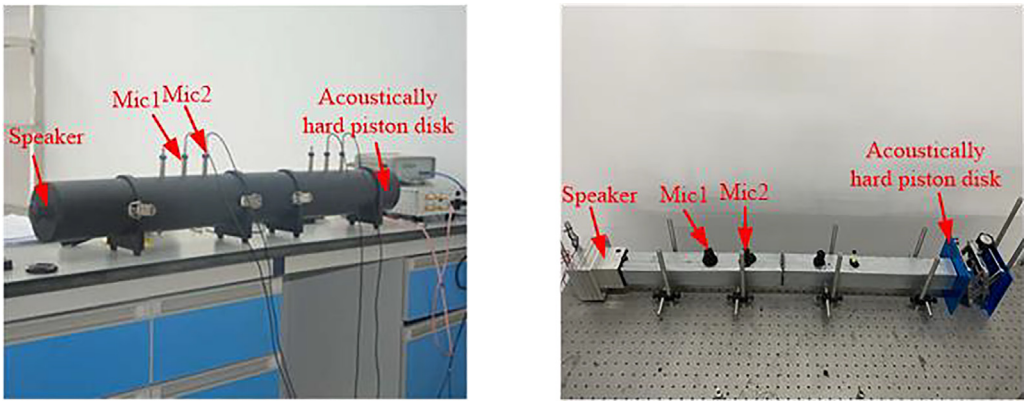

Fig. 14. Sound impedance tube test platform. (a) B&K type-4206 impedance tube system; (b) square impedance tube system.

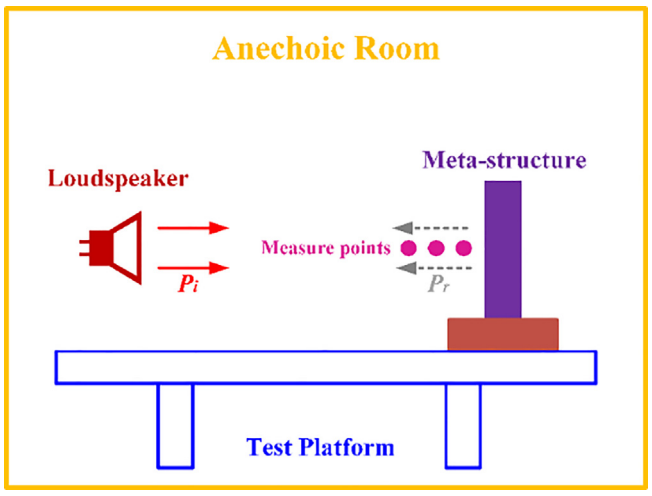

Fig. 15. Schematic of anechoic room experimental platform.

absorption units in Table 3 and Table 4, respectively. Moreover, compared with the sound absorption performance of case 2, where the acoustic critical effect is not considered in the structural design, the sound absorption performance of case 1 is significantly better. Specifically, in the frequency range of 1200 Hz-2600 Hz, the sound absorption performance of case 1 is 30 % higher than that of case 2, and the difference between the two cases becomes more obvious after 2000 Hz.

In order to obtain a more accurate sound absorption performance in the high-frequency range, Fig. 16(b) provides the sound absorption coefficient of case 3 and case 4 obtained by the square impedance tube experiment. The difference between the theoretical results and the experimental results is caused by the processing error in the 3D printing process of the samples. The sound absorption coefficient of case 3, which considered acoustic critical absorption effect and applied uniform arrangement is higher than that of case 4. This phenomenon demonstrates the significance of the acoustic critical absorption effect on the high-frequency band and the optimization of the structural absorption performance. Furthermore, comparing Fig. 16(a) and 16(b) can see that the influence of acoustic critical sound absorption effect is reduced, which can be seen from the increase of sound absorption coefficient shown in the two figures. This is attributed to the reduction of the sound incident area. Therefore, the acoustic critical absorption effect has greater influence on sound absorption structure with larger cross-sectional area and wider frequency range.

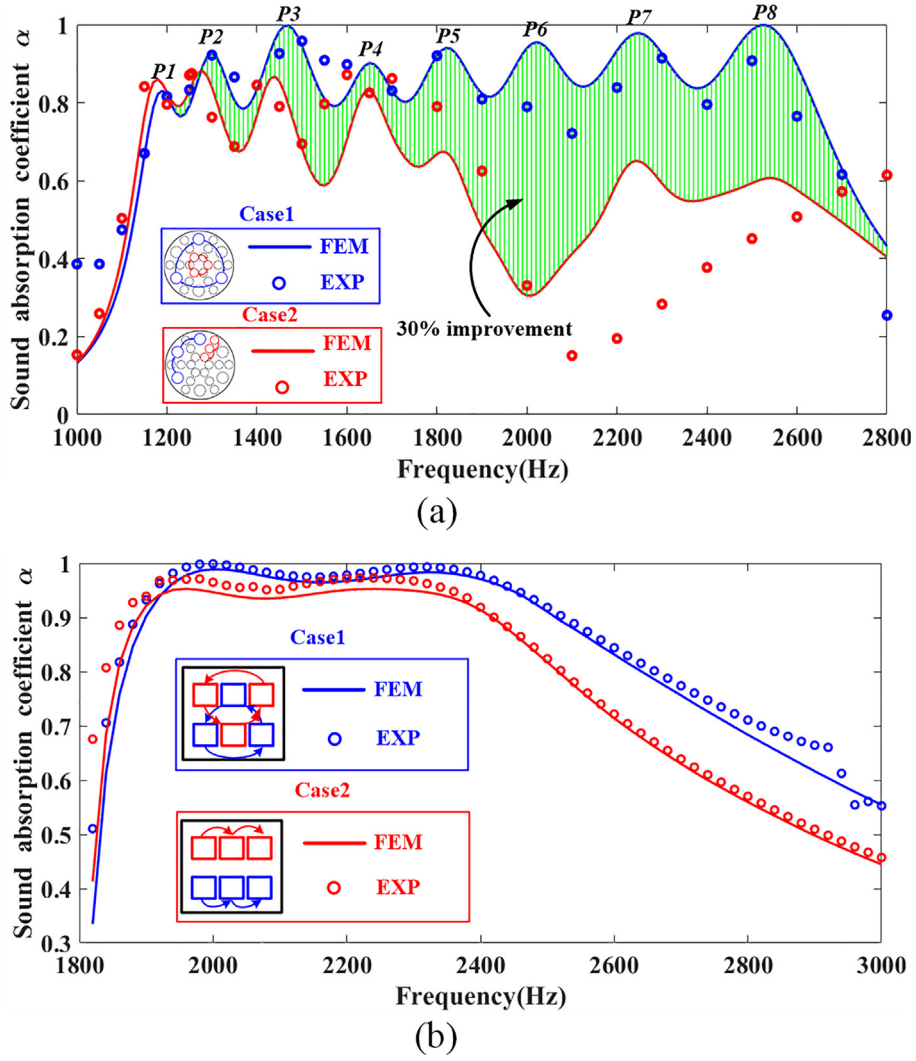

Fig. 16. Sound absorption performance of 4 meta-structures. (a) sound absorption performance of case 1 and case 2; (b) sound absorption performance of case 3 and case 4.

4.3. Research implications and prospects

Firstly, from the mechanism perspective, the purpose of designing the frequency band of the structure as 1000–2800 Hz in this paper is to highlight the acoustic critical absorption effect rather than only play a role in the high-frequency band. This idea also supports the structural design of low-frequency sound absorption with a thickness of 50 mm.

Secondly, from the technology perspective, the mechanism proposed in this paper can be applied to micro-perforated panels and other resonant-type structures, so it has strong realizability and stability in structure preparation technology. However, some foam materials have high preparation technology requirements and great performance uncertainty.

Thirdly, from the application perspective, although many types of foams with 50 mm thickness can provide the same sound absorption performance or even better, they still have some limitations, such as unstable performance at high temperature, high pressure, and after prolonged use. The high production price is also a disadvantage limiting its application. Our work can complement the limitations of foam and has engineering application value.

Finally, since the acoustic critical absorption effect has a greater impact on structures with larger cross-sectional area and wider frequency range, this paper can provide a reliable guarantee for the broadband efficient design of meta-absorbers with multiple parallel arranged subunits.

5. Conclusions

This paper provides general guidance for optimizing sound absorption performance of finite size resonant-type structures from the perspective of unit layout. On this basis, both finite element calculation and experiment results verified that the meta-structure with 24 units that applied the proposed rules could achieve a 30 % higher average sound absorption coefficient than those not applied. For unit arrangement of the structure, there are three main rules: firstly, the effective sound absorption area of the resonant unit is a limited circle area, and its diameter decreases with the resonance frequency increase. When the sum of the influential sound absorption area of the resonant units at its corresponding resonance frequency is equal to the cross-sectional area of the meta-structure, the meta-structure can achieve perfect sound absorption at this frequency; secondly, when multiple units with the same resonant frequency are arranged in parallel, the distance between them should be greater than or equal to the effective sound absorption diameter. Thus, a peak with a perfect absorption coefficient is obtained instead of several peaks with low absorption coefficients; lastly, for multiple units with different resonance frequencies, the units with lower resonance frequencies should be arranged on the inner and outer sides of the structure, and the units with higher resonance frequencies should be arranged in the middle part of the structure. The results of this paper can be directly applied to the design of meta-absorbers composed by multiple parallel arranged subunits, and has potential applications in architectural acoustics product design and vibration and noise reduction of industrial equipment.

CRediT authorship contribution statement

Li Bo Wang: Conceptualization, Methodology, Software. **Chang Wang:** Visualization, Software. **Yun Zhong Lei:** Methodology. **Shao Kun Yang:** Writing – review & editing. **Jiu Hui Wu:** Funding acquisition, Writing – review & editing.

Data availability

Data will be made available on request.

Declaration of Competing Interest

The authors declare that they have no known competing financial interests or personal relationships that could have appeared to influence the work reported in this paper.

References

[1] Bianchi S, Corsini A, Sheard AG. A critical review of passive noise control techniques in industrial fans. J Eng Gas Turbines Power Trans Asme 2014.
[2] Arjunan A, Wang C, English M, Stanford M, Lister P. A computationally-efficient numerical model to characterize the noise behavior of metal-framed walls. Metals 2015;5(3):1414–31.
[3] Gus'kov, Yu S, Cipriani M, De Angelis R, Consoli F, Rupasov AA, Andreoli P. Absorption coefficient for nanosecond laser pulse in porous material. Plasma Phys Contr F 2015;57(12):125004.
[4] Huang K, Yang D, He S. Acoustic absorption properties of open-cell Al alloy foams with graded pore size. J Phys D Appl Phys 2011;44:365405.
[5] Dias T, Monaragala R. Sound absorbtion in knitted structures for interior noise reduction in automobiles. Meas Sci Technol 2006;17(9):2499.
[6] Arenas JP, Darmendrail L. Measuring sound absorption properties of porous materials using a calibrated volume velocity source. Meas Sci Technol 2013;24 (10):105005.
[7] Yang J, Lee JS, Kim YY. Multiple slow waves in metaporous layers for broadband sound absorption. J Phys D Appl Phys 2017;50:015301.
[8] Xie ZK, Ikeda T, Okuda Y, Nakajima H. Characteristics of sound absorption in lotus-type porous magnesium. Jpn J Appl Phys 2004;43(10):7315–9.
[9] Ning JF, Ren SW, Zhao GP. Acoustic properties of micro-perforated panel absorber having arbitrary cross-sectional perforations. Appl Acoust 2016;111 (OCT.):135–42.
[10] Jung SS, Kim YT, Lee DH. Sound absorption of micro-perforated panel. J Korean Phys Soc 2007;50(4):1044–51.
[11] Arjunan A. Acoustic absorption of passive destructive interference cavities. Mater Today Commun 2019;19:68–75.
[12] Liu L, Hussein MI. Wave motion in periodic flexural beams and characterization of the transition between Bragg scattering and local resonance. Int J Appl Mech 2012;79(1):1003.
[13] Arjunan A, Baroutaji A, Robinson J. Advances in acoustic metamaterials. Encyclopedia of Smart Materials 2021;3:1–10.
[14] Arjunan A, Baroutaji A, Robinson J, Wang C. Characteristics of acoustic metamaterials. Encyclopedia of Smart Materials 2022;3:35–45.
[15] Gil M, Bonache J and Selga J. Broadband Resonant-Type Metamaterial Transmission Lines IEEE Microw. Wirel. Co. 2007; 17:97-99.
[16] Cheng BZ, Gao NS, Zhang RH, Hou H. Design and experimental investigation of broadband quasi-perfect composite loaded sound absorber at low frequencies. Appl Acoust 2021;178:108026.
[17] Yang Z, Mei J, Yang M, Chan NH, Sheng P. Membrane-type acoustic metamaterial with negative dynamic mass. Phys Rev Lett 2008;101 (20):204301–4.
[18] Mei J, Ma G, Yang M, Yang Z, Wen W, Sheng P. Dark acoustic metamaterials assuper absorbers for low-frequency sound. Nat Commun 2012;3(2):756–7.
[19] Chen Y, Huang G, Zhou X, Hu G, Sun C-T. Analytical coupled vibroacoustic modeling of membrane-type acoustic metamaterials: plate model. J Acoust Soc Am 2014;136(6):2926–34.
[20] Langfeldt F, Riecken J, Gleine W, Von Estorff O. A membrane-type acoustic metamaterial with adjustable acoustic properties. J Sound Vib 2016;373:1–18.
[21] Ma G, Yang M, Xiao S, Yang Z, Sheng P. Acoustic metasurface with hybrid resonances. Nat Mater 2014;13(9):873–8.
[22] Ma F, Huang M, Wu JH. Acoustic metamaterials with synergetic coupling. J Appl Phys 2017;122(21):215102–8.
[23] Leblanc A, Lavie A. Three-dimensional-printed membrane-type acoustic metamaterial for low frequency sound attenuation. J Acoust Soc Am. 017; 104(6):EL538–42.
[24] Almeida G, Vergara EF, Barbosa LR. Low-frequency sound absorption of a metamaterial with symmetrical-coiled-up spaces. Appl Acoust 2021;172:107593.
[25] Wang Y , Zhao H , Yang H. A tunable sound-absorbing metamaterial based on coiled-up space. J Appl Phys 2018; 123(18):185109.1-185109.6.
[26] Wu F, Xiao Y, Yu D. Low-frequency sound absorption of hybrid absorber based on micro-perforated panel and coiled-up channels. Appl Phys Lett 2019;114 (15):151901.
[27] Ni X, Wu Y, Chen ZG. Acoustic rainbow trapping by coiling up space. Sci Rep 2014;4(7446):7038.
[28] Mousavi SH, Khanikaev AB, Wang Z. Topologically protected elastic waves in phononic metamaterials. Nat commun 2015;6:8682.
[29] Zhu R, Liu XN, Hu GK. Negative refraction of elastic waves at the deep-subwavelength scale in a single-phase metamaterial. Nat Commun 2014;5:5510.
[30] Arjunan A, Baroutaji A, Latif A. Acoustic behaviour of 3D printed titanium perforated panels. Results Eng 2021:100252.
[31] Gao N, Tang L, Deng J. Design, fabrication and sound absorption test of composite porous metamaterial with embedding I-plates into porous polyurethane sponge. Appl Acoust 2021;175:107845.

[32] Liu CR, Wu JH. A thin multi-order Helmholtz metamaterial with perfect broadband acoustic absorption. Appl Phys Express 2019;12(8):084002.
[33] Loganathan Y, Jeyanthi S. Acoustic performance of countersunk micro-perforated panel in multilayer porous material. Build Acoust 2019:27(6).
[34] Zhang XJ, Zhao XD. Multilayer micro perforated panel optimization design. J Audio Eng Soc 2008.
[35] Ma F, Huang M, Wu JH. Ultrathin lightweight plate-type acoustic metamaterials with positive lumped coupling resonant. J Appl Phys 2017;121(1):015102.
[36] Liu CR, Wu JH, Lu K, et al. Acoustical siphon effect for reducing the thickness in membrane-type metamaterials with low-frequency broadband absorption. Appl Acoust 2019;148:1–8.
[37] Huang SB, Zhou ZL, Li DT, et al. Compact broadband acoustic sink with coherently coupled weak resonances. Sci Bull 2020;15:373–9.
[38] Zhou Z L, Huang S B, Li D T et al. Broadband impedance modulation via non-local acoustic metamaterials. Natl. Sci. Rev. 2021.
[39] Ding H, Wang N Y, Qiu S et al. Broadband acoustic meta-liner with metal foam approaching causality-governed minimal thickness. Int. J. Mech. Sci. 2022.
[40] Zhou YK, Li DT, Li Y, Hao T. Perfect acoustic absorption by subwavelength metaporous composite. Appl Phys Lett 2019;115:093503.
[41] Gao NS, Zhang ZC. Optimization design and experimental verification of composite absorber with broadband and high efficiency sound absorption. Appl Acoust 2021;183:108288.
[42] Maa DY. Potential of microperforated panel absorber. J Acoust Soc Am 1998;104(5):2861–6.
[43] ISO 15034-2:1998(E). Acoustics-Determination of sound absorption coefficient and impedance in impedance tubes 1998.
[44] Ma F, Wang C, Du Y, Zhu Z, Wu JH. Enhancing of broadband sound absorption through soft matter. Mater Horiz 2022;9:653–62.